Interplay of turbulence and proton-microinstability growth in space plasmas

Cite as: Phys. Plasmas **29**, 102107 (2022); https://doi.org/10.1063/5.0098625
Submitted: 11 May 2022 • Accepted: 20 September 2022 • Published Online: 27 October 2022

Riddhi Bandyopadhyay, Ramiz A. Qudsi, S. Peter Gary, et al.

Physics of Plasmas ARTICLE scitation.org/journal/php

Interplay of turbulence and proton-microinstability growth in space plasmas

Cite as: Phys. Plasmas **29**, 102107 (2022); doi: 10.1063/5.0098625
Submitted: 11 May 2022 · Accepted: 20 September 2022 ·
Published Online: 27 October 2022

Riddhi Bandyopadhyay,[1,a] Ramiz A. Qudsi,[2] S. Peter Gary,[3,b] William H. Matthaeus,[4,5] Tulasi N. Parashar,[4,5] Bennett A. Maruca,[4,5] Vadim Roytershteyn,[3,b] Alexandros Chasapis,[6] Barbara L. Giles,[7] Daniel J. Gershman,[7] Craig J. Pollock,[8] Christopher T. Russell,[9] Robert J. Strangeway,[9] Roy B. Torbert,[10] Thomas E. Moore,[7] and James L. Burch[11]

AFFILIATIONS

[1]Department of Astrophysical Sciences, Princeton, New Jersey 08544, USA
[2]Center for Space Physics, Boston University, Boston, Massachusetts 02215, USA
[3]Space Science Institute, Boulder, Colorado 80301, USA
[4]Department of Physics and Astronomy, University of Delaware, Newark, Delaware 19716, USA
[5]Bartol Research Institute, Newark, Delaware 19716, USA
[6]Laboratory for Atmospheric and Space Physics, University of Colorado Boulder, Boulder, Colorado 80303, USA
[7]NASA Goddard Space Flight Center, Greenbelt, Maryland 20771, USA
[8]Denali Scientific, Fairbanks, Alaska 99709, USA
[9]University of California, Los Angeles, California 90095-1567, USA
[10]University of New Hampshire, Durham, New Hampshire 03824, USA
[11]Southwest Research Institute, San Antonio, Texas 78238-5166, USA

[a]**Author to whom correspondence should be addressed:** riddhib@princeton.edu
[b]Deceased.

ABSTRACT

Numerous prior studies have shown that as proton beta increases, a narrower range of proton temperature anisotropy values is observed. This effect has often been ascribed to the actions of kinetic microinstabilities because the distribution of observational data aligns with contours of constant instability growth rates in the beta-anisotropy plane. However, the linear Vlasov theory of instabilities assumes a uniform background in which perturbations grow. The established success of linear-microinstability theories suggests that the conditions in regions of extreme temperature anisotropy may remain uniform for a long enough time so that the instabilities have the chance to grow to sufficient amplitude. Turbulence, on the other hand, is intrinsically nonuniform and nonlinear. Thin current sheets and other coherent structures generated in a turbulent plasma may quickly destroy the uniformity. It is, therefore, not a-priori obvious whether the presence of intermittency and coherent structures favors or disfavors instabilities. To address this question, we examined the statistical distribution of growth rates associated with proton temperature-anisotropy driven microinstabilities and local nonlinear time scales in turbulent plasmas. Linear growth rates are, on average, substantially less than the local nonlinear rates. However, at the regions of extreme values of temperature anisotropy, near the "edges" of the populated part of the proton temperature anisotropy-parallel beta plane, the instability growth rates are comparable or faster than the turbulence time scales. These results provide a possible answer to the question as to why the linear theory appears to work in limiting plasma excursions in anisotropy and plasma beta.

I. INTRODUCTION

The interplanetary plasma typically exhibits weak collisionality and strong turbulence.[1,2] Similar conditions exist in many astrophysical systems. In such high-temperature, low-density magnetized plasmas, Coulomb collisions between particles are rare, which allows the velocity distribution function (VDF) of a given particle species to persist in a state far from local thermodynamic equilibrium. Consequently, the VDFs are generally non-Maxwellian, and the distortions of the VDFs

are manifested through substantial anisotropy in the pressure (or, equivalently, temperature) tensor. Distorted VDFs can give rise to plasma microinstabilities[3] that can strongly influence dynamics, a topic that has received considerable attention recently.[4–6] However, it is known that these distortions are themselves often caused, or amplified, by intermittency in the form of coherent structures, generated by nonlinearity in turbulent dynamics.[7,8] Intermittency is also responsible for faster local turbulence time scales. This implies a competition between linear and nonlinear processes, necessarily involving enhancements of each due to intermittency. These effects have not been taken into account in previous treatments of the problem;[4,6,9] it is this competition that we address in the present paper.

A simple VDF that exhibits temperature anistropy is the bi-Maxwellian, which has been extensively used is the plasma theory literature. In this model, the VDF is characterized by well-defined distinct temperatures $T_{\perp j}$ and $T_{\|j}$ for species j, referred to the directions perpendicular and parallel to the magnetic field. The anisotropy of j-particles is then quantified by the ratio

$$R_{\rm j} = \frac{T^{\rm j}_{\perp}}{T^{\rm j}_{\|}}. \tag{1}$$

Although deviations from equilibrium are observed in all charged plasma species,[10–12] here we focus on protons. The extreme values of proton-temperature anisotropy in the solar wind exhibit a strong dependence on the parallel-proton beta,[13–15]

$$\beta_{\|\rm p} = \frac{n_{\rm p}\, k_{\rm B}\, T^{\rm p}_{\|}}{B_0^2 / (2\,\mu_0)}, \tag{2}$$

where $n_{\rm p}$ is the proton number density, $k_{\rm B}$ is the Boltzmann constant, and μ_0 is the permeability of vacuum. For progressively larger $\beta_{\|\rm p}$ values, the range of observed temperature-anisotropy values narrows in the solar wind[14] and the terrestrial magnetosheath.[16]

Kinetic microinstabilities[3] offer an appealing theoretical explanation for the observed correlation between temperature anisotropy and plasma beta. Linearization of the Vlasov–Maxwell system about an assumed anisotropic equilibrium predicts that for extreme values of $R_{\rm p}$ and $\beta_{\|\rm p}$, the distribution function becomes unstable, triggering the growth of waves. It is typically assumed that upon reaching finite amplitude, these fluctuations drive the plasma toward (temperature) isotropy. The initial growth rate of the unstable waves is derivable via linear theory from the values of $\beta_{\|\rm p}$ and $R_{\rm p}$.

An important question is whether the unstable waves produced in this way are merely a passive "side effect," or if they actively modify the dynamics. Some authors adopt the interpretation that the ion-driven microinstabilities may "feed" strong fluctuations[17] in regions of instability, materially impacting the plasma dynamics. A different point of view is that turbulence-cascade generated localized inhomogeneities, i.e., coherent structures such as current sheets,[8,18] drive the temperature-anisotropies to extreme values, setting the stage for linear instabilities that might occur in regions of strong nonlinear effects. Indeed recent studies such as He *et al.*[19] have shown in detail that velocity distributions are deformed by kinetic activity near intense current sheets, thus driving plasma activity such as the firehose instability, which subsequently enhances turbulence.

The dissipation of turbulent fluctuations in weakly collisional space plasmas involves the transfer of fluctuation energy from field and flow energies to thermal energies. The processes that contribute to this dissipation generally fall into one of two categories: strongly nonlinear intermittent processes well represented by particle-in-cell simulations and microinstability processes typically computed by linear dispersion theory in homogeneous plasmas. The electrons are treated as fluid in hybrid simulations. Within the limited scope of hybrid simulations, turbulence and microinstabilitites have been shown to coexist.[20–22]

Indeed, strong fluctuations are found near the same extreme regions of the $\beta_{\|\rm p}, R_{\rm p}$-plane where the instability growth rates are large, causing the plasma to remain (marginally) unstable to temperature-anisotropy instabilities.[17,23,24] Similarly, computations of shear-driven turbulence[25] have shown that local instabilities can sporadically arise due to kinetic effects that are inevitably found near current sheets and vortices.[18,26] From these studies, it is evident that regions contributing to strong intermittency are also regions of strong kinetic activity, and furthermore, these are often juxtaposed. It remains unclear, which type of process—linear or nonlinear—dominates on average and determines the dynamics of large-scale phenomena. One may study this relationship by comparing the relative time scales of nonlinear and linear dynamical processes.[6,27] There is some subtlety in this comparison when the medium is inhomogeneous, in that intermittency enters this comparison in a significant way, while the standard instability calculation that we employ assumes extended plane wave solutions.

Recent studies of turbulence-driven cascade and temperature-anisotropy driven microinstability[6,22,27] find that the majority of solar-wind intervals, in an idealized situation, would support the proton-driven microinstabilities. However, the associated growth rates are rarely faster than all the other relevant time scales. Quantitatively, the nonlinear time scales, estimated from the spectral amplitude near the ion-inertial scale, are faster than the growth rates for most of the analyzed samples. This comparison suggests that the turbulent cascade quickly destroys the ideal situation for harboring micro-instabilities, which would, otherwise, grow to macroscopic values as unstable modes.

As suggested above, the important physics of intermittency[28] motivates modification of results obtained from globally based estimates such as *average* nonlinear time or *average* spectral amplitude near a given scale. Intermittent structures occupy a small fraction of the volume, but are likely responsible for a large fraction of the plasma heating and particle energization.[29] Keeping this in mind, we propose that, instead of comparing timescales based on average fluctuation amplitude with growth rates, it is reasonable to compare the two based on the corresponding local values of plasma and turbulence properties.

To address the above issues, here we carry out a local analysis of both the instability growth rates and the nonlinear time scales. We analyze three datasets:

(1) A three-dimensional, kinetic, particle-in-cell (PIC) simulation,
(2) *in situ* observations of Earth's magnetosheath by the *MMS* spacecraft, and
(3) *in situ* observation of the interplanetary solar wind by the *Wind* spacecraft.

For all three cases, we will show that both instability growth rates and nonlinear rates are intermittent with enhanced values near coherent structures,[23,30] and that, pointwise, the nonlinear processes are faster than the instabilities for a majority of cases.

II. THEORY AND METHOD

A. Linear Vlasov theory

Solving the dispersion relation for the linearized Vlasov and Maxwell's equations in a homogeneous plasma, one obtains the angular frequencies, ω, associated with a given wavevector $\mathbf{k}$. The imaginary component of ω is the growth or decay rate of the $\mathbf{k}$ mode. The dominant growth rate of a particular instability, expected in linear theory to trigger macroscopic effects, is

$$\gamma_{\max} \equiv \max_{\mathbf{k}} \Im(\omega), \tag{3}$$

where the maximum operation is taken over all wave-vectors $\mathbf{k}$ associated with that instability. The plasma is considered unstable to a given instability if $\gamma_{\max} > 0$.

To calculate these growth rates, the technique and software of Refs. 16 and 31 are employed. For each pair of $(\beta_{\parallel p}, R_p)$-values, the value of $\gamma_{\max}$ is determined for each of the four instabilities by computing the maximum value of $\Im(\omega)$ over a range of $\mathbf{k}$-values. For every point with $\gamma_{\max} > 0$, we select the maximum growth rate from the four types of instabilities, associated with proton-temperature anisotropy,

$$\Gamma_{\max} = \max\{\gamma_{\max}^{\text{cyclotron}}, \gamma_{\max}^{\text{mirror}}, \gamma_{\max}^{\parallel-\text{firehose}}, \gamma_{\max}^{\parallel-\text{firehose}}\}, \tag{4}$$

where each term inside the bracket represents the maximum growth rate for the corresponding instability, i.e., the cyclotron, mirror, parallel firehose and oblique firehose instabilities, respectively, as indicated by the superscript. Values of $\Gamma_{\max}$ less than $10^{-5}\,\Omega_p$ are taken to be 0 (i.e., effectively stable). Note that in strong turbulence the plasma parameters vary significantly in space, so a separate calculation of $\Gamma_{\max}$ is required at each point $\mathbf{r}$.

B. Nonlinear timescales

The local nonlinear timescale, at a position $\mathbf{r}$, for a lengthscale ℓ can be estimated as

$$\tau_{\text{nl}}(\mathbf{r}) \sim \ell/\delta b_\ell, \tag{5}$$

where the longitudinal magnetic field increment is

$$\delta b_\ell = |\hat{\ell} \cdot [\mathbf{b}(\mathbf{r}+\ell) - \mathbf{b}(\mathbf{r})]| \tag{6}$$

and $\mathbf{b}$ is the total magnetic field expressed in Alfvén speed units. The vector lag ℓ has a magnitude ℓ and direction $\hat{\ell}$. The timescale $\tau_{\text{nl}}(\mathbf{r})$ is a strongly varying function of position and may take on large values near coherent structures. This local estimate of nonlinear time is generalized from Kolmogorov's estimate of the average nonlinear timescale which is given, at wavenumber k, by $\tau_{\text{nl}}(k) = 1/(ku_k) \sim 1/(k\sqrt{E(k)})$. Accordingly, we compare the local values of γ and τ_{nl}.

For comparison with instability growth rates, it is convenient to compute an equivalent frequency from the nonlinear timescales as $\omega_{\text{nl}} = 2\pi/\tau_{\text{nl}}$. Although majority of highly unstable modes are found to have the associate wavenumber close to the ion-inertial length (d_i), to carefully evaluate the nonlinear frequency at the scale of the fastest growing mode and to account for the statistical spread in the associated wavenumber $k_{\max}$ we use a variable increment scale with

$$\ell = 1/k_{\max}, \tag{7}$$

where $k_{\max}$ is the wavenumber associated with the fastest growing mode (separately for each point), as recently done by Klein *et al.*[9]

III. PIC SIMULATION

We analyze data obtained from a three-dimensional, fully kinetic, particle-in-cell (PIC) simulation.[32] The simulation has 2048^3 grid points, with $L = 41.9\,d_i$, $\beta_p = \beta_e = 0.5$, $m_p/m_e = 50$, $\delta B/B_0 = 1$. The analysis is performed on a snapshot late in time evolution of the simulation. For more details, refer to Ref. 32. We emphasize that no attempt is made to closely align the simulation parameters with those of the magnetosheath or the solar wind. The three systems have very different plasma parameters, such as turbulence amplitude, plasma beta, and Reynolds number. A different initial condition in the simulation would have led to possibly different outcomes, but the three systems together cover plasma regimes rather broadly.

Figure 1 shows the estimated values of probability density of $(\beta_{\parallel p}, R_p)$-values in the 3D PIC data, along with the contours of

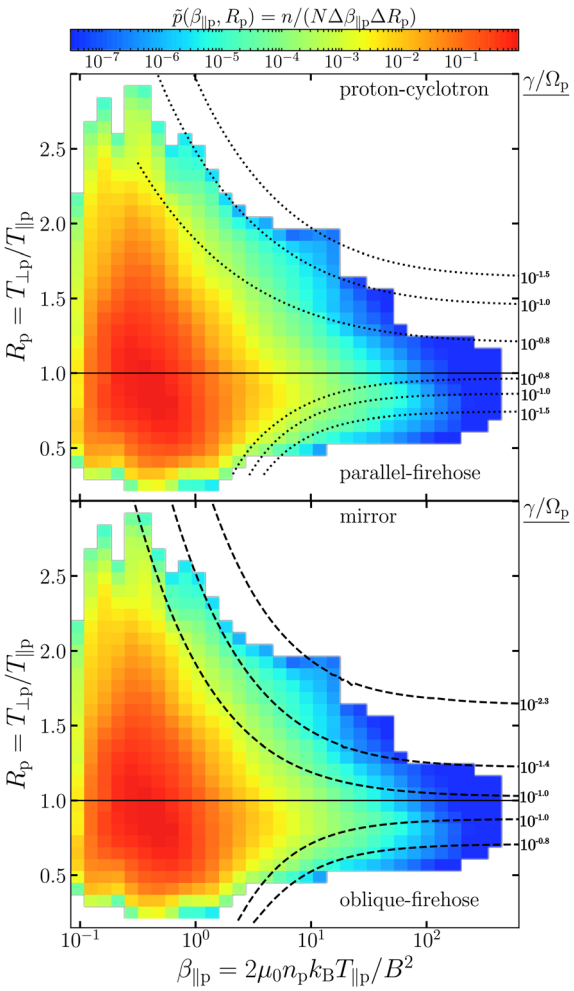

FIG. 1. Two plots of the estimated probability density, $\tilde{p}$, of $(\beta_{\parallel p}, R_p)$-values for the 3D PIC data. The two panels are identical except for the overlaid curves, which show contours of constant growth rate for different instabilities. The curves in the top panel show the parallel instabilities: the proton-cyclotron ($R_p > 1$) and parallel-firehose ($R_p < 1$). The curves in the bottom panel show the oblique instabilities: the mirror ($R_p > 1$) and oblique-firehose ($R_p < 1$). Each contour is labeled with its growth rate, γ, in units of the proton cyclotron frequency, Ω_p.

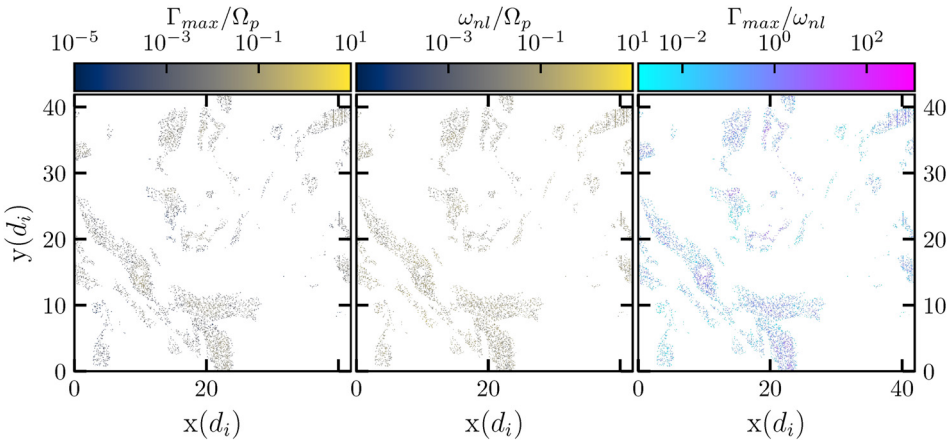

FIG. 2. Plots (from left to right) of maximum growth rate Γ_{max}, nonlinear frequency ω_{nl} evaluated for a lag of $\ell = 1/k_{max}$, and the ratio Γ_{max}/ω_{nl} at $z \approx 35.6\, d_i$ from PIC simulation.

constant instability growth rate, indicating involvement of $\beta_{\|p}$-dependent constraints on R_p, in the simulation data. Although, for any given $\beta_{\|p}$-value, a distribution of R_p-values is observed, the distribution's center occurs near $R_p \approx 1$, and its width becomes progressively narrower with increased $\beta_{\|p}$. Thus, the plasma likely hosts processes that favor isotropic proton-temperatures (limiting both $R_p > 1$ and $R_p < 1$), and these processes likely become more active at higher values of $\beta_{\|p}$. We believe these are the first reports of such $\beta_{\|p}$-dependent constraints on R_p in a three-dimensional, fully kinetic PIC simulation. Similar plots are obtained for the solar wind[31] and magnetosheath.[16]

The left panel of Fig. 2 shows the distribution of maximum growth rate, Γ_{max} [Eq. (4)], for a plane perpendicular to the mean magnetic field, at $z \approx 35.6\, d_i$. The center panel illustrates the nonlinear frequencies at each point, averaged over lags of $\ell = 1/k_{max}$ along the x, y, and z directions. From the first two panels of Fig. 2, it is evident that both kinds of frequencies are distributed intermittently in space, with clusters of large values in similar regions. However, from the right panel, the ratio of these frequencies rarely exceeds unity. Even if both kind of processes are enhanced near the same regions of physical space, the nonlinear processes are typically faster. Although Fig. 2 plots only one plane, later we show an analysis from the full 3D simulation domain.

In situ observation—Though our analysis with the PIC simulations has important implications, the PIC simulation carries several limitations, e.g., artificial proton to electron mass ratio, small system size. Therefore, we next perform similar analyses, for two naturally occurring turbulent plasma systems: Earth's magnetosheath and the interplanetary solar wind.

We use burst-mode *MMS*[33] data sampled in the Earth's magnetosheath for several burst-mode periods in both quasi-parallel and quasi-perpendicular shocked plasmas, including the ones reported in Ref. 16. The *MMS*/Fast Plasma Investigation[34] moments provide $\beta_{\|p}$, R_p-values and magnetic-field measurements from the flux gate magnetometer[35] are used to compute the longitudinal increment [Eq. (5)] at a spatial separation of $\ell = 1/k_{max}$. We select the magnetosheath intervals where the flow speed is greater than the Alfvén speed and use the Taylor hypothesis to convert the temporal separation to spatial separation ($\ell = -\langle|\mathbf{V}|\rangle\tau$). The nonlinear frequencies were computed from the magnetic-field increments and interpolated to the ion cadence of 150 ms. The instability growth rates are calculated at ion cadence from the $\beta_{\|p}$, R_p values.

The specific intervals of MMS data that we analyze are the same as those reported in Ref. 16. The final statistics, shown later, are accumulated from all the intervals. However, in Fig. 3, we show, as an example, a 40 min burst-mode sample from 06:12:43 to 06:52:23 UTC

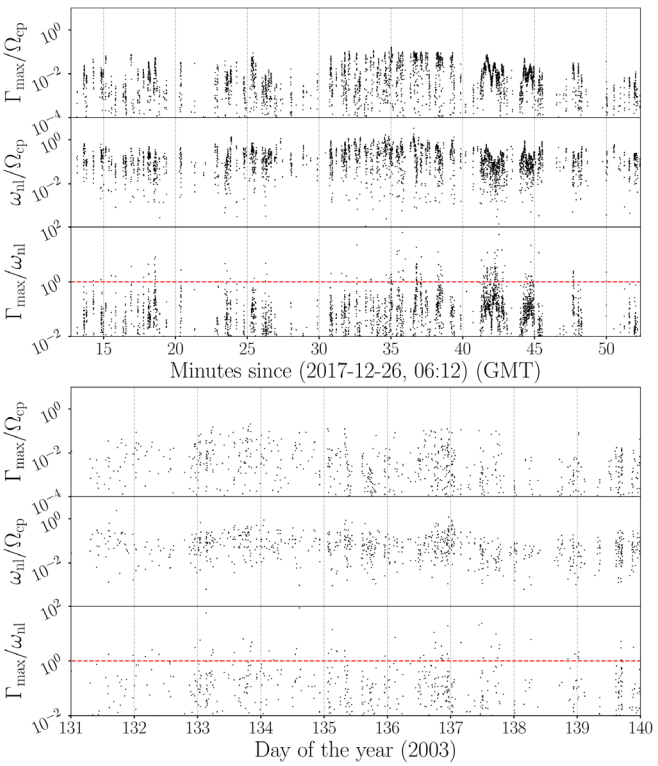

FIG. 3. Time series of the maximum instability growth rates Γ_{max} (top), the nonlinear frequency ω_{nl} at $\ell = 1/k_{max}$ (middle), and the ratio Γ_{max}/ω_{nl} (bottom) for a burst-mode magnetosheath sample observed by the *MMS* spacecraft (top) and an interplanetary solar wind interval sampled by the *Wind* spacecraft (bottom). Note that due to the large difference in the measurement resolution of the *MMS* and *Wind* spacecraft, the time scales in the two figures are vastly different (~40 min vs ~10 days); however, they contain a similar number of correlation times of the respective data.

TABLE I. Fraction of points with $\Gamma_{max} > \omega_{nl}$ for different systems.

	3DPIC	MMS	Wind
Number of points with $\Gamma_{max}/\omega_{nl} > 1$	11%	4%	12%

on 26 December 2017. Note that this interval is typical and not chosen for any special properties, other that the preliminary observation that it is turbulent and contains current sheets.[30,36] The bottom panel on the top plot of Fig. 3 clearly shows that the ratio Γ_{max}/ω_{nl} for this interval rarely exceeds unity. The fraction of points for which the instability rate is greater than the nonlinear rate are given in Table I.

In the bottom plot of Fig. 3, we show a similar analysis for 1 au solar wind. The *Wind* data used here are identical to those reported in Ref. 31. We use measurements from *Wind* satellite, accumulated over a period of about ten days. We use 11 Hz magnetic field measurements from *Wind*'s Magnetic Field Investigation[37] to calculate ω_{nl} for a Taylor-shifted separation of $\ell = 1/k_{max}$. The two Faraday cups in the Solar Wind Experiment[38] return one ion spectrum every ≈90 s and the ω_{nl} values are interpolated to this cadence. A bi-Maxwellian distribution is fit to each ion spectrum to compute proton moments[39] and, thus, infer values of R_p and $\beta_{\|p}$. In the small sample of ≈10 days of *Wind* data, shown in the bottom plot of Fig. 3, the exhibited behavior closely resembles the magnetosheath results (Fig. 3, top), apart from the differences in time scales. Again, the nonlinear frequency, ω_{nl}, is greater than the instability growth rate, γ, for the majority, and the regions in which the growth rate is of relative significance are sporadic.

A key result of this paper is shown in Fig. 4. Here, we plot joint probability distribution functions of the instability growth rates (Γ_{max}) and the nonlinear frequencies (ω_{nl}) for all three datasets. These plots represent a concise but compelling way of comparing linear theory results against nonlinear results, while at the same time enabling a comparison of observations vs simulations. Note that all the rates are normalized by the respective cyclotron frequency, allowing direct comparison. In all three cases, the core of the distribution resides well below the $\Gamma_{max} = \omega_{nl}$ line. From this result, we see that for most data samples, the nonlinear processes are faster than the linear-instability growth, when the substantial nonuniformity, or intermittency, of both types of processes are taken into account.

All of the datasets show that nonlinear time scales are, in general, faster than the fastest of the linear timescales. This suggests that in most cases the linear instabilities do not have enough time to grow in the plasma in a way that is significant enough to affect the dynamics or the statistical behavior of whole plasma.

On the other hand, decades of studies indicate that linear theory is effective in predicting the boundaries of $(\beta_{\|p}, R_p)$-plots, which suggest that linear instabilities regulate extreme values of R_p. To explore this, we look at the distribution of the two frequencies (Γ_{max} and ω_{nl}) and their ratio for the three datasets (PIC, MMS, and Wind) on the $(\beta_{\|p}, R_p)$-plane. Figure 5 shows this ratio in the three cases. Here, we can see that the region along the edges, which is most susceptible to instability is where most of the instability is present. For all the three cases, the ratio of the two frequencies is increasing as we move outside from the centroid of the distribution. In all three cases, the linear time scales become comparable or faster than their nonlinear counterpart near the edges of the $(\beta_{\|p}, R_p)$-plots. This result shows that although in majority of the plasma Γ_{max} is less than ω_{nl}, it is greater than ω_{nl} along the periphery of the populated part of the $(\beta_{\|p}, R_p)$-plane. Consideration of this pattern may explain how the instabilities are quite efficient at limiting the extension of the plasma population to extreme anisotropy regions.

We note that the boundaries from $\Gamma_{max}/\omega_{nl} < 1$ to $\Gamma_{max}/\omega_{nl} > 1$ in the $(\beta_{\|p}, R_p)$-plane are very similar in all three panels. These critical lines signify the effectiveness of nonlinear vs linear processes in the plasmas. The similarity in the lines in all the three graphs suggests that the transition occurs in a similar manner in all cases. The pattern of the MMS data is notably less extended than the other two cases. One possibility to explain this is the generally greater level of turbulence in the magnetosheath. There are other potential explanations as well, including factors such as degree of compressibility, differing system size, nature of driving, etc. Exploration of these differences is beyond the current scope of the study.

IV. DISCUSSION AND CONCLUSIONS

Temperature-anisotropy driven microinstabilities are often considered to constrain the temperature anisotropy values in weakly collisional plasmas.[14,15,40] Recall that the linear Vlasov theory of instabilities assumes a homogeneous background, in which background a small perturbation grows exponentially. The established success of linear-microinstability theories suggests that the conditions near the extremely anisotropic temperature may be uniform enough to justify an application of homogeneous linear theories. Turbulence, on the other hand, is intrinsically nonuniform and nonlinear. Thin current sheets, and other coherent structures generated by the energy

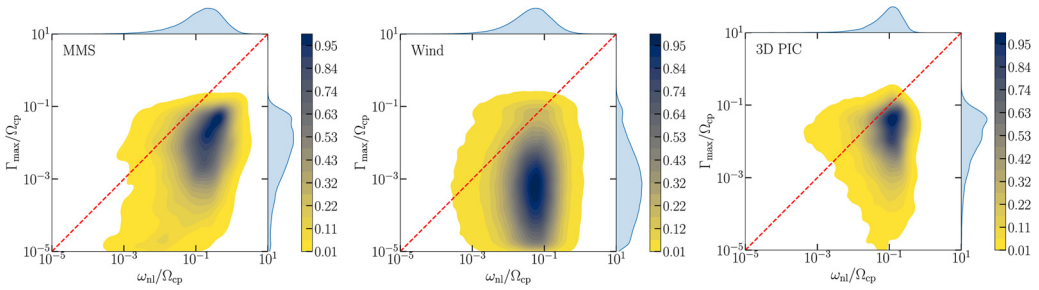

FIG. 4. Joint probability distribution functions of the maximum instability growth rate Γ_{max} and the nonlinear frequency ω_{nl} from PIC simulation, *MMS* data in the magnetosheath, and *Wind* data in the interplanetary solar wind. The fraction of points above the $\Gamma_{max} = \omega_{nl}$ line is about 4% for the MMS data, 12% for the Wind data, and 11% for the 3D PIC data. Only $\gamma > 0$ cases are considered here. This is further discussed in Sec. IV.

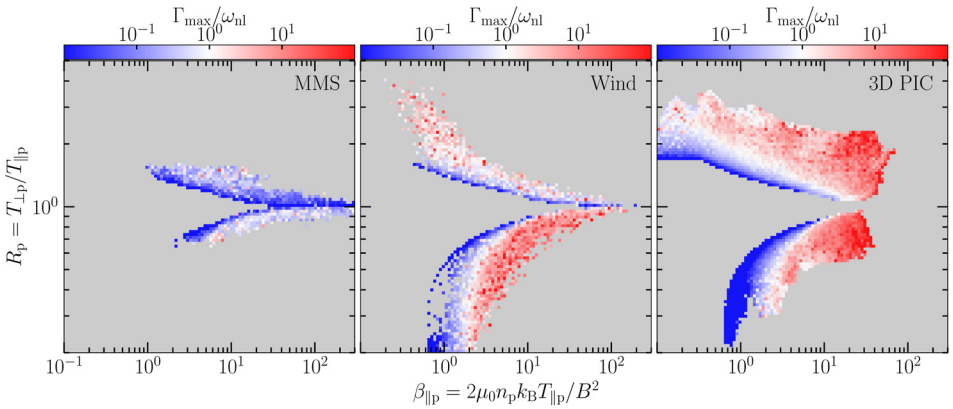

FIG. 5. Distribution of the ratio of the maximum linear growth rate (Γ_{max}) to the nonlinear frequency (ω_{nl}) evaluated at the wavenumber of maximum growth rate on the ($\beta_{\parallel p}, R_p$) -plane for the three cases.

cascade, are sites of extreme temperature anisotropy,[18] and therefore, the high growth rates due to the microinstabilities also reside in the same vicinity. It is, therefore, not *a priori* obvious whether the presence of intermittency and coherent structures favors or disfavors instabilities in comparison with nonlinear effects. This question has motivated the present study.

To address this question, we have examined the statistical distribution of growth rates associated with proton temperature-anisotropy driven microinstabilities and the local nonlinear time scales in three distinct systems. The three systems cover different ranges of $(R_p, \beta_{\parallel p})$-values among other parameters. However, both simulation and observation results show that, when the comparison is performed in this way, locally in space, only a small fraction of the samples support long-lived linear instabilities. Naively, one may conclude that the nonlinear effects do not allow sufficient time for the instabilities to grow large enough to affect the global dynamics to any significant degree (Fig. 4). Yet, decades of observations present strong evidence that linear microinstabilities regulate ion temperature anisotropy. A number of studies using *in situ* observations (e.g., Refs. 13–16, and 31), have found that the distribution of plasma over the $(R_p, \beta_{\parallel p})$-plane is well restricted by the thresholds predicted by linear Vlasov theory. The results shown in Fig. 1 provide further evidence.

Figure 5 presents a partial resolution of this apparent contradiction between linear and nonlinear processes. We see that although $\omega_{nl} > \Gamma_{max}$ for most data, linear instabilities do become faster and possibly even disrupt the turbulence cascade at most extreme anisotropies, for which microkinetic instabilities are expected to be most active.

Klein *et al.*[6] find that about 50% of all cases are unstable, and less than 10% of those cases have growth rates faster than the nonlinear time. We find that the fraction of data points with $\gamma > 0$ is about 28% for the MMS data, 16% for the Wind data, and 16% for the 3D PIC data, Within the set of unstable points about 4% for the MMS data and 12% for the Wind data, and 11% for the 3D PIC data show $\Gamma_{max} > \omega_{nl}$. These differences are likely due to our use of a *local* nonlinear time as well as our approximation of the VDFs as bi-Maxwellian.

These illuminating results motivate further studies that incorporate more sophisticated analyses. In particular, the present study utilized several simplifying assumptions. This work has assumed that ion VDFs are well modeled as bi-Maxwellians. Though this is often the case for the "core" portion, the full VDF frequently exhibits a "beam" and/or other features. Each of these additional non-Maxwellian features can modify the free energy available to drive instabilities, thus modifying the computed growth rates (e.g., Ref. 41). Furthermore, the fluctuation growth rates or dissipation rates estimated by linear theory are often less than that measured in practice (see Refs. 42 and 43). The approach suggested by He *et al.*[42,43] might lead to a greater range of applicability of linear theory associated with taking into account many unstable waves. Including such refinements would represent a significant extension of the present study.

ACKNOWLEDGMENTS

We dedicate this article to the memory of our co-author S. Peter Gary. Throughout his illustrious career—which included literally writing the book on microinstabilities in space plasmas—he remained a tireless, insightful collaborator and a patient, supportive mentor to many in the field.

T.N.P. was supported by NSF SHINE Grant No. AGS-1460130 and NASA HGI Grant No. 80NSSC19K0284. W.H.M. is a member of the *MMS* Theory and Modeling Team and was supported by NASA Grant No. NNX14AC39G. The research of S.P.G. was supported by NASA Grant No. NNX17AH87G.

The simulation described in this paper was performed as a part of the Blue Waters sustained-petascale computing project, which was supported by the National Science Foundation (Award Nos. OCI-0725070 and ACI-1238993) and the State of Illinois. Blue Waters allocation was provided by NSF PRAC Award No. 1614664.

The authors would like to thank Rohit Chhiber for useful discussions and Yan Yang for helping to prepare the PIC dataset.

AUTHOR DECLARATIONS

Conflict of Interest

The authors have no conflicts to disclose.

Author Contributions

Riddhi Bandyopadhyay: Conceptualization (equal); Data curation (equal); Formal analysis (equal); Funding acquisition (supporting); Investigation (equal); Methodology (equal); Resources (equal); Writing – original draft (equal). **Daniel J. Gershman:** Writing – review & editing (equal). **Craig J. Pollock:** Writing – review & editing

(equal). **Christopher Thomas Russell:** Writing – review & editing (equal). **Robert J. Strangeway:** Writing – review & editing (equal). **Roy Torbert:** Writing – review & editing (equal). **Thomas E Moore:** Writing – review & editing (equal). **James Leo Burch:** Writing – review & editing (equal). **Ramiz Qudsi:** Formal analysis (equal); Methodology (equal); Validation (equal); Writing – review & editing (equal). **S. P. Gary:** Conceptualization (equal); Funding acquisition (equal); Investigation (equal); Writing – review & editing (equal). **William H. Matthaeus:** Conceptualization (lead); Funding acquisition (lead); Investigation (equal); Methodology (equal); Supervision (lead); Writing – original draft (equal). **Tulasi Nandan Parashar:** Conceptualization (equal); Formal analysis (equal); Funding acquisition (equal); Investigation (equal); Methodology (equal); Resources (equal); Software (equal); Supervision (equal); Validation (equal). **Bennett Maruca:** Conceptualization (equal); Formal analysis (equal); Methodology (equal); Supervision (equal); Validation (equal); Writing – review & editing (equal). **Vadim Roytershteyn:** Formal analysis (equal); Methodology (equal); Writing – review & editing (equal). **Alexandros Chasapis:** Investigation (equal); Methodology (equal); Writing – review & editing (equal). **Barbara L. Giles:** Writing – review & editing (equal).

DATA AVAILABILITY

This study used Level 2 FPI and FIELDS data according to the guidelines set forth by the *MMS* instrumentation team. All data are freely available at https://lasp.colorado.edu/MMS/sdc/, Refs. 33–35. We thank the *MMS* SDC, FPI, and FIELDS teams for their assistance with this study. *Wind* SWE and MFI data are available from CDAWeb (https://cdaweb.gsfc.nasa.gov/), Refs. 37 and 38. The authors thank the *Wind* team for the *Wind* magnetic field and plasma data.

The bi-Maxwellian analysis code is summarized in Ref. 39.

REFERENCES

[1]R. Bruno and V. Carbone, "The solar wind as a turbulence laboratory," Living Rev. Sol. Phys. **2**, 4 (2005).
[2]G. Zimbardo, A. Greco, L. Sorriso-Valvo, S. Perri, Z. Vörös, G. Aburjania, K. Chargazia, and O. Alexandrova, "Magnetic turbulence in the geospace environment," Space Sci. Rev. **156**, 89–134 (2010).
[3]S. P. Gary, *Theory of Space Plasma Microinstabilities* (Cambridge University Press, Cambridge, 1993).
[4]S. D. Bale, J. C. Kasper, G. G. Howes, E. Quataert, C. Salem, and D. Sundkvist, "Magnetic fluctuation power near proton temperature anisotropy instability thresholds in the solar wind," Phys. Rev. Lett. **103**, 211101 (2009).
[5]B. A. Maruca, J. C. Kasper, and S. D. Bale, "What are the relative roles of heating and cooling in generating solar wind temperature anisotropies?," Phys. Rev. Lett. **107**, 201101 (2011).
[6]K. G. Klein, B. L. Alterman, M. L. Stevens, D. Vech, and J. C. Kasper, "Majority of solar wind intervals support ion-driven instabilities," Phys. Rev. Lett. **120**, 205102 (2018).
[7]A. Greco, W. H. Matthaeus, R. D'Amicis, S. Servidio, and P. Dmitruk, "Evidence for nonlinear development of magnetohydrodynamic scale intermittency in the inner heliosphere," Astrophys. J. **749**, 105 (2012).
[8]S. Servidio, F. Valentini, D. Perrone, A. Greco, F. Califano, W. H. Matthaeus, and P. Veltri, "A kinetic model of plasma turbulence," J. Plasma Phys. **81**, 325810107 (2015).
[9]K. G. Klein, M. Martinović, D. Stansby, and T. S. Horbury, "Linear stability in the inner heliosphere: Helios re-evaluated," Astrophys. J. **887**, 234 (2019).
[10]W. G. Pilipp, H. Miggenrieder, M. D. Montgomery, K.-H. Mühlhäuser, H. Rosenbauer, and R. Schwenn, "Characteristics of electron velocity distribution functions in the solar wind derived from the HELIOS plasma experiment," J. Geophys. Res.: Space Phys. **92**, 1075–1092, https://doi.org/10.1029/JA092iA02p01075 (1987).
[11]M. Maksimovic, I. Zouganelis, J.-Y. Chaufray, K. Issautier, E. E. Scime, J. E. Littleton, E. Marsch, D. J. McComas, C. Salem, R. P. Lin, and H. Elliott, "Radial evolution of the electron distribution functions in the fast solar wind between 0.3 and 1.5 AU," J. Geophys. Res.: Space Phys. **110**, A09104, https://doi.org/10.1029/2005JA011119 (2005).
[12]E. Marsch, "Kinetic physics of the solar corona and solar wind," Living Rev. Sol. Phys. **3**, 1 (2006).
[13]S. P. Gary, R. M. Skoug, J. T. Steinberg, and C. W. Smith, "Proton temperature anisotropy constraint in the solar wind: ACE observations," Geophys. Res. Lett. **28**, 2759–2762, https://doi.org/10.1029/2001GL013165 (2001).
[14]J. C. Kasper, A. J. Lazarus, and S. P. Gary, "Wind/SWE observations of firehose constraint on solar wind proton temperature anisotropy," Geophys. Res. Lett. **29**, 20-1–20-4, https://doi.org/10.1029/2002GL015128 (2002).
[15]P. Hellinger, P. Trávníček, J. C. Kasper, and A. J. Lazarus, "Solar wind proton temperature anisotropy: Linear theory and WIND/SWE observations," Geophys. Res. Lett. **33**, L09101, https://doi.org/10.1029/2006GL025925 (2006).
[16]B. A. Maruca, A. Chasapis, S. P. Gary, R. Bandyopadhyay, R. Chhiber, T. N. Parashar, W. H. Matthaeus, M. A. Shay, J. L. Burch, T. E. Moore, C. J. Pollock, B. J. Giles, W. R. Paterson, J. Dorelli, D. J. Gershman, R. B. Torbert, C. T. Russell, and R. J. Strangeway, "MMS observations of beta-dependent constraints on ion temperature-anisotropy in Earth's magnetosheath," Astrophys. J. **866**, 25 (2018).
[17]S. D. Bale, P. J. Kellogg, F. S. Mozer, T. S. Horbury, and H. Reme, "Measurement of the electric fluctuation spectrum of magnetohydrodynamic turbulence," Phys. Rev. Lett. **94**, 215002 (2005).
[18]A. Greco, F. Valentini, S. Servidio, and W. H. Matthaeus, "Inhomogeneous kinetic effects related to intermittent magnetic discontinuities," Phys. Rev. E **86**, 066405 (2012).
[19]H. Jiansen, Z. Xingyu, C. Yajie, S. Chadi, S. Michael, L. Hui, R. Wenzhi, Z. Lei, and T. Chuanyi, "Plasma heating and Alfvénic turbulence enhancement during two steps of energy conversion in magnetic reconnection exhaust region of solar wind," Astrophys. J. **856**, 148 (2018).
[20]M. W. Kunz, A. A. Schekochihin, and J. M. Stone, "Firehose and mirror instabilities in a collisionless shearing plasma," Phys. Rev. Lett. **112**, 205003 (2014).
[21]S. A. Markovskii, B. J. Vasquez, and B. D. G. Chandran, "Proton temperature-anisotropy instability coexisting with ambient turbulence in the solar-wind plasma," Astrophys. J. **875**, 125 (2019).
[22]P. Hellinger, L. Matteini, S. Landi, L. Franci, A. Verdini, and E. Papini, "Turbulence vs. fire hose instabilities: 3-D hybrid expanding box simulations," e-print arXiv:1908.07760 (2019).
[23]K. T. Osman, W. H. Matthaeus, B. Hnat, and S. C. Chapman, "Kinetic signatures and intermittent turbulence in the solar wind plasma," Phys. Rev. Lett. **108**, 261103 (2012).
[24]S. Servidio, K. T. Osman, F. Valentini, D. Perrone, F. Califano, S. Chapman, W. H. Matthaeus, and P. Veltri, "Proton kinetic effects in Vlasov and solar wind turbulence," Astrophys. J. **781**, L27 (2014).
[25]H. Karimabadi, V. Roytershteyn, M. Wan, W. H. Matthaeus, W. Daughton, P. Wu, M. Shay, B. Loring, J. Borovsky, E. Leonardis, S. C. Chapman, and T. K. M. Nakamura, "Coherent structures, intermittent turbulence, and dissipation in high-temperature plasmas," Phys. Plasmas **20**, 012303 (2013).
[26]T. N. Parashar and W. H. Matthaeus, "Propinquity of current and vortex structures: Effects on collisionless plasma heating," Astrophys. J. **832**, 57 (2016).
[27]W. H. Matthaeus, S. Oughton, K. T. Osman, S. Servidio, M. Wan, S. P. Gary, M. A. Shay, F. Valentini, V. Roytershteyn, H. Karimabadi, and S. C. Chapman, "Nonlinear and linear timescales near kinetic scales in solar wind turbulence," Astrophys. J. **790**, 155 (2014).
[28]W. H. Matthaeus, M. Wan, S. Servidio, A. Greco, K. T. Osman, S. Oughton, and P. Dmitruk, "Intermittency, nonlinear dynamics and dissipation in the solar wind and astrophysical plasmas," Philos. Trans. R. Soc. A **373**, 20140154 (2015).
[29]M. Wan, W. H. Matthaeus, V. Roytershteyn, T. N. Parashar, P. Wu, and H. Karimabadi, "Intermittency, coherent structures and dissipation in plasma turbulence," Phys. Plasmas **23**, 042307 (2016).
[30]R. A. Qudsi, R. Bandyopadhyay, B. A. Maruca, T. N. Parashar, W. H. Matthaeus, A. Chasapis, S. P. Gary, B. L. Giles, D. J. Gershman, C. J. Pollock, R. J. Strangeway, R. B. Torbert, T. E. Moore, and J. L. Burch, "Intermittency

and ion temperature–anisotropy instabilities: Simulation and magnetosheath observation," Astrophys. J. **895**, 83 (2020).
[31]B. A. Maruca, J. C. Kasper, and S. P. Gary, "Instability-driven limits on helium temperature anisotropy in the solar wind: Observations and linear Vlasov analysis," Astrophys. J. **748**, 137 (2012).
[32]V. Roytershteyn, H. Karimabadi, and A. Roberts, "Generation of magnetic holes in fully kinetic simulations of collisionless turbulence," Philos. Trans. R. Soc. A **373**, 20140151 (2015).
[33]J. L. Burch, T. E. Moore, R. B. Torbert, and B. L. Giles, "Magnetospheric multiscale overview and science objectives," Space Sci. Rev. **199**, 5–21 (2016).
[34]C. Pollock, T. Moore, A. Jacques, J. Burch, U. Gliese, Y. Saito, T. Omoto, L. Avanov, A. Barrie, V. Coffey, J. Dorelli, D. Gershman, B. Giles, T. Rosnack, C. Salo, S. Yokota, M. Adrian, C. Aoustin, C. Auletti, S. Aung, V. Bigio, N. Cao, M. Chandler, D. Chornay, K. Christian, G. Clark, G. Collinson, T. Corris, A. De Los Santos, R. Devlin, T. Diaz, T. Dickerson, C. Dickson, A. Diekmann, F. Diggs, C. Duncan, A. Figueroa-Vinas, C. Firman, M. Freeman, N. Galassi, K. Garcia, G. Goodhart, D. Guererro, J. Hageman, J. Hanley, E. Hemminger, M. Holland, M. Hutchins, T. James, W. Jones, S. Kreisler, J. Kujawski, V. Lavu, J. Lobell, E. LeCompte, A. Lukemire, E. MacDonald, A. Mariano, T. Mukai, K. Narayanan, Q. Nguyan, M. Onizuka, W. Paterson, S. Persyn, B. Piepgrass, F. Cheney, A. Rager, T. Raghuram, A. Ramil, L. Reichenthal, H. Rodriguez, J. Rouzaud, A. Rucker, Y. Saito, M. Samara, J.-A. Sauvaud, D. Schuster, M. Shappirio, K. Shelton, D. Sher, D. Smith, K. Smith, S. Smith, D. Steinfeld, R. Szymkiewicz, K. Tanimoto, J. Taylor, C. Tucker, K. Tull, A. Uhl, J. Vloet, P. Walpole, S. Weidner, D. White, G. Winkert, P.-S. Yeh, and M. Zeuch, "Fast plasma investigation for magnetospheric multiscale," Space Sci. Rev. **199**, 331–406 (2016).
[35]C. T. Russell, B. J. Anderson, W. Baumjohann, K. R. Bromund, D. Dearborn, D. Fischer, G. Le, H. K. Leinweber, D. Leneman, W. Magnes, J. D. Means, M. B. Moldwin, R. Nakamura, D. Pierce, F. Plaschke, K. M. Rowe, J. A. Slavin, R. J. Strangeway, R. Torbert, C. Hagen, I. Jernej, A. Valavanoglou, and I. Richter, "The magnetospheric multiscale magnetometers," Space Sci. Rev. **199**, 189–256 (2016).
[36]T. N. Parashar, A. Chasapis, R. Bandyopadhyay, R. Chhiber, W. H. Matthaeus, B. Maruca, M. A. Shay, J. L. Burch, T. E. Moore, B. L. Giles, D. J. Gershman, C. J. Pollock, R. B. Torbert, C. T. Russell, R. J. Strangeway, and V. Roytershteyn, "Kinetic range spectral features of cross helicity using the magnetospheric multiscale spacecraft," Phys. Rev. Lett. **121**, 265101 (2018).
[37]R. P. Lepping, M. H. Acūna, L. F. Burlaga, W. M. Farrell, J. A. Slavin, K. H. Schatten, F. Mariani, N. F. Ness, F. M. Neubauer, Y. C. Whang, J. B. Byrnes, R. S. Kennon, P. V. Panetta, J. Scheifele, and E. M. Worley, "The wind magnetic field investigation," Space Sci. Rev. **71**, 207–229 (1995).
[38]K. W. Ogilvie, D. J. Chornay, R. J. Fritzenreiter, F. Hunsaker, J. Keller, J. Lobell, G. Miller, J. D. Scudder, E. C. Sittler, R. B. Torbert, D. Bodet, G. Needell, A. J. Lazarus, J. T. Steinberg, J. H. Tappan, A. Mavretic, and E. Gergin, "SWE, a comprehensive plasma instrument for the wind spacecraft," Space Sci. Rev. **71**, 55–77 (1995).
[39]B. A. Maruca and J. C. Kasper, "Improved interpretation of solar wind ion measurements via high-resolution magnetic field data," Adv. Space Res. **52**, 723–731 (2013).
[40]D. Verscharen, K. G. Klein, and B. A. Maruca, "The multi-scale nature of the solar wind," Living Rev. Sol. Phys. **16**, 5 (2019).
[41]M. M. Martinović, K. G. Klein, T. Ďurovcová, and B. L. Alterman, "Ion-driven instabilities in the inner heliosphere. I. Statistical trends," Astrophys. J. **923**, 116 (2021).
[42]J. He, D. Duan, T. Wang, X. Zhu, W. Li, D. Verscharen, X. Wang, C. Tu, Y. Khotyaintsev, G. Le, and J. Burch, "Direct measurement of the dissipation rate spectrum around ion kinetic scales in space plasma turbulence," Astrophys. J. **880**, 121 (2019).
[43]J. He, X. Zhu, D. Verscharen, D. Duan, J. Zhao, and T. Wang, "Spectra of diffusion, dispersion, and dissipation for kinetic Alfvénic and compressive turbulence: Comparison between kinetic theory and measurements from MMS," Astrophys. J. **898**, 43 (2020).